applied sciences

MDPI

Article

Development of 5-DOF Piezoelectric Actuator for Planar—Angular Positioning

Andrius Čeponis [1,*], Vytautas Jūrėnas [1] and Dalius Mažeika [2]

[1] Robotics and Piezomechanics Laboratory, Institute of Mechatronics, Kaunas University of Technology, K. Donelaičio Str. 73, LT-44249 Kaunas, Lithuania; vytautas.jurenas@ktu.lt
[2] Department of Information Systems, Faculty of Fundamental Sciences, Vilnius Gediminas Technical University, Saulėtekio al. 11, LT-10223 Vilnius, Lithuania; dalius.mazeika@vgtu.lt
* Correspondence: andrius.ceponis@ktu.lt

Abstract: A novel five degrees of freedom (5-DOF) piezoelectric actuator is proposed and analyzed in this paper. The actuator can provide unlimited self-motion in the plane and angular positioning of the spherical payload. The actuator is composed of a cylindrical bronze frame and a piezo ceramic ring glued on top of the cylinder. The cylinder has three cut-outs used to form three supports. The top electrode of the piezo ceramic ring is divided into six equal sections. Three electrodes are used to control the direction of the planar motion, while the remaining three electrodes allow controlling angular motion. The planar motion of the actuator is induced by employing radial vibrations of the supports, while the rotational motion of the sphere is obtained when radial vibrations of the corresponding sections of the piezo ceramic ring are excited. The proposed design of the actuator allows reducing coupling between vibrations of the different segments and ensures the possibility to obtain 5-DOF motion. The piezoelectric actuator is excited using a single harmonic signal switched between electrodes via a digitally controlled switch box. The numerical and experimental studies of the actuator were performed, and the operating principle was validated. The maximum linear velocity of 19.8 mm/s and angular speed of 31.3 RPM were obtained when the payload of 55.68 g and excitation voltage of 200 $V_{p\text{-}p}$ was applied.

Keywords: planar motion; angular motion; piezoelectric actuator; five degrees of freedom

Citation: Čeponis, A.; Jūrėnas, V.; Mažeika, D. Development of 5-DOF Piezoelectric Actuator for Planar—Angular Positioning. *Appl. Sci.* **2022**, *12*, 1033. https://doi.org/10.3390/app12031033

Academic Editor: Jörg Wallaschek

Received: 29 November 2021
Accepted: 13 January 2022
Published: 20 January 2022

1. Introduction

Modern high-precision mechatronic positioning systems use different types of actuators, i.e., electromagnetic, electrostatic, and magnetostrictive. However, most of the actuators are a single degree of freedom devices that generate linear or rotary motion [1]. Usually, in order to induce multiple degrees of freedom motion of the particular type, several actuators are composed into one complex positioning system [2–4]. Such a design principle makes the overall design and control of the positioning system complex and bulky [5,6]. Moreover, the synchronization of several actuators is a challenging control task that requires expensive and complex control electronics and software. In addition, synchronization and control of the system consisting of several actuators decrease the accuracy and reliability of positioning systems [7,8]. Therefore, multi-DOF actuators must be used to simplify control of multi-degree of freedom positioning systems and to reduce the size and complexity of the mechatronic systems. Piezoelectric actuators can induce multi DOF motion of the slider or rotor, have a simple design, self-locking option, short response time, and good controllability [9,10]. Numerous designs of multi-DOF piezoelectric actuators have been proposed [11–14]. However, most of them operate only as linear type, rotational type, or can move itself in the plane. In order to combine two types of motion into one piezoelectric system, several piezoelectric actuators must be composed, and the aforementioned disadvantages will be met again [15,16]. Therefore, the objective of this research is to develop a multi-DOF locomotion type piezoelectric actuator consisting of

a single transducer that is able to provide unlimited self-motion in the plane and rotate spherical payload.

Hernando-Garcia et al. introduced a piezoelectric robot with the ability to generate bi-directional in-plane motion [17]. The proposed robot has a simple design and operation principle, i.e., the body of the robot is based on a millimeter size glass plate with two piezoelectric patches, while the operation of it is based on the generation of the traveling wave, which is obtained at a frequency that is between frequencies of two bending modes. The authors performed numerical and experimental investigations and found that the proposed robot is able to provide up to 100 mm/s of planar speed while the amplitude of the excitation signal was equal to 65 $V_{p\text{-}p}$. On the other hand, the proposed robot is able to provide only one type of motion, i.e., planar, while generation of rotary motion is not foreseen.

Su et al. introduced planar motion quadruped piezoelectric micro-robot [18]. The robot design is based on four piezoelectric legs, which are bonded to a rectangle base. The planar motion of the robot is obtained by the excitation of two perpendicular bending modes of the legs. In order to obtain the elliptical motion trajectory of the legs, two harmonic signals with phase differences were used, and as a result, planar motion is obtained. Numerical and experimental investigations were performed and showed that the proposed robot is able to provide 33.45 mm/s of planar speed and convey up to 200 g of payload.

Numerous different designs of piezoelectric robots that can provide planar motion are proposed and investigated [19,20]. However, most of these piezorobots cannot provide more than three degrees of freedom. On the other hand, several authors introduced 2-DOF rotary—linear piezoelectric actuators that can rotate and provide linear motion of the slider.

Mashimo and Toyama reported on a rotary—linear piezoelectric actuator [21]. The actuator consists of a single cubic stator with a cylindrical cavity inside. Dimensions of the actuator can be minimized up to millimeter size. Linear or rotary motion of cylindrical slider can be obtained when the third radial or hybrid vibrations of the first and second extension modes of the stator are excited. An experimental study showed that an actuator can achieve an angular velocity of 24 rad/s and a linear speed of 80 mm/s. However, the clamping problem of the actuator, as well as the preloading and wearing problems of the slider, are not solved.

Tundecemir et al. introduced a dual-function rotary—linear actuator consisting of a cylinder type transducer with slanted piezo ceramic plates [22]. Linear or rotational motion of the cylindrical transducer is excited employing vibrations of the first longitudinal mode or of the first torsional vibration modes of the cylinder using saw-tooth type signal. The angular velocity of 3 rad/s and linear velocity of 5 mm/s was obtained. It must be noted that the range of the linear motion of the transducer is limited by the length of the cylinder.

Han et al. reported on the rotary—linear actuator that has a piezoelectric tube with helical electrodes [23]. The actuator operation principle is based on the excitation of the first longitudinal and the first torsional vibration modes. A saw-tooth waveform electric signal is used for actuator driving. The actuator provides a linear velocity of 2.4 mm/s and angular velocity of 9.9×10^5 μrad/s. However, the range of linear motion is limited.

Literature review showed that most of the dual-function actuators provide rotary and linear motion of cylinder-type sliders. Also, no found planar locomotion actuator or piezorobot that can rotate payload and operate as 5DOF actuators were found. Therefore, this research aimed to propose and investigate a novel design of the 5DOF self-motion piezoelectric actuator that can provide unlimited locomotion in the plane and rotary motion of the spherical payload. The main novelty of the actuator is that mechanical translation and rotation are induced using a single piezoelectric ring. Such a design principle allows achieving planar or angular motion using a particular resonant frequency, while the direction of motion is controlled by switching harmonic electric signals between electrodes of the ring. The novel design of the cylindrical frame allows efficiently decoupling vibrations of the particular zones and to achieve planar motion or rotation of the spherical payload independently.

The rest of the paper is organized as follows. Section 2 describes the structure, dimensions, and operation principle of the novel actuator. Also, excitation schematics of the electrodes are described. Section 3 presents the results of numerical modeling. Section 4 provides measured characteristics of the actuator, i.e., the dependence of the angular and linear velocity from applied voltage and payload. Finally, Section 5 concludes this work.

2. Design and Operation Principle of the Actuator

The actuator is composed of a cylindrical frame and a piezoceramic ring glued on top of the cylinder (Figure 1). The frame is made from beryllium bronze C17200, while ring material is hard piezoceramic PIC181 (PI Ceramics, Lederhose, Germany). The spherical payload is placed on the top of the ring. The top electrode of the piezo ceramic ring is divided into six equal sections. The beryllium bronze cylinder has three cut-outs used to form three supports and to make six sectors along the circumference of the cylinder. The length of these sectors and their position corresponds with the length and position of the electrodes. The three supports are used to transfer vibrations of the piezo ceramic ring to the contact zone and to induce planar motion of the whole actuator on basis of vibro-impact principle. The other three sections are used to generate rotations of the spherical payload about three axes. It must be mentioned that there are an additional six cuts made in the cylinder used to separate six zones of the cylinder. These additional cuts reduce the vibration coupling of different zones of the actuator. In addition, alumina oxide spherical contacts are glued at the bottom of the supports and on the top of the piezo ceramic ring in each zone. Spherical contacts ensure higher friction force between contacting surfaces and allow to locate them on the antinodes of the particular vibration mode. The design of the actuator is shown in Figure 1, while Figure 2 and Table 1 represent geometrical characteristics.

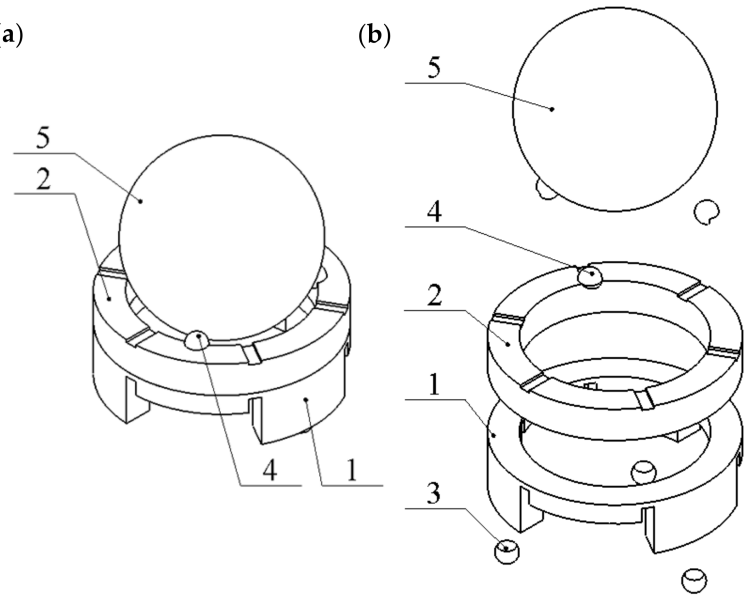

Figure 1. Design of the actuator: (**a**)—assembled view; (**b**)—exploited view; 1—beryllium bronze cylinder; 2—piezoceramic ring; 3—spherical contacts used for linear motion; 4—spherical contacts used for angular motion; 5—spherical payload.

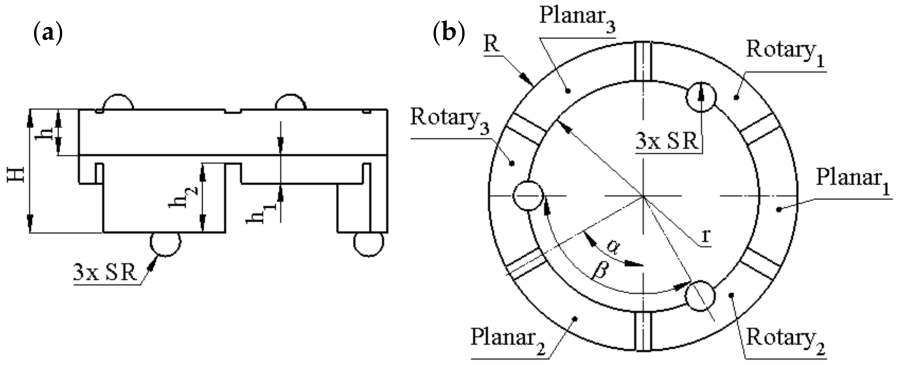

Figure 2. Sketch of the actuator: (**a**)—side view; (**b**)—top view; $Planar_1$–$Planar_3$ are sections of piezo ceramic ring dedicated to controlling planar motion; $Rotary_1$–$Rotary_3$ are sections of piezo ceramic ring used to control the rotary motion of the payload.

Table 1. Geometrical parameters of the actuator.

Parameter	Value	Description
R	10 mm	The outer radius of the actuator
r	7.5 mm	The inner radius of the actuator
SR	1 mm	The spherical radius of alumina oxide contacts
H	8 mm	Total height of the actuator
h	3 mm	Height of piezo ceramic ring
h_1	1.8 mm	Height of seismic mass
h_2	4.5 mm	Height of support
α	60°	Angular value of electrode segment
β	120°	Angle between spherical contacts

The piezoelectric actuator has a simple design and can be scaled. The introduced actuator occupies a 2.99 cm^3 space together with the spherical payload. The total mass of the actuator without payload is 12.55 g.

The operation principle of the actuator is based on the excitation of the two vibration modes, i.e., the first radial vibration mode of the supports and the third radial vibration mode of the piezo ceramic ring. A single harmonic signal is used to excite a particular motion of the actuator. If one of the $Planar_1$–$Planar_3$ electrodes (Figure 2) located above the support is excited by harmonic signal at the resonant frequency of the first radial mode of the support, then the linear motion of the actuator is induced into the normal direction of the support.

Reverse linear motion of the actuator is obtained when the other two $Planar_1$–$Planar_2$ electrodes are excited by harmonic signal with the same frequency. In order to generate angular motion of spherical payload, one of the sections dedicated to controlling angular motion ($Rotary_1$–$Rotary_3$) should be affected by harmonic signal with frequency equal to the natural frequency of the third radial mode of piezo ceramic ring. Reverse motion is obtained by exciting two opposite electrodes. All three $Rotary_1$–$Rotary_3$ segments must be affected by three harmonic signals with a phase difference of 120° to obtain rotation of the payload about the *Z*-axis. It should be noted that preload of the actuator induced by spherical payload affects vibration amplitudes of the actuator. Therefore, the difference between amplitudes of the active and passive zones of the actuator is increased. This allows reducing disturbance in the motion direction when the particular electrode is affected.

Motion control of the actuator was implemented using two harmonic signals with different frequencies that are controlled by two independent digitally controlled switch boxes (Table 2). The planar motion of the actuator or rotary motion of the payload is excited by switching on or off corresponding switches. The excitation scheme is given in Figure 3, while Table 1 presents the control signals for switching boxes that are used to obtain a particular motion.

Table 2. Switching between electrodes used for motion direction control.

Motion Direction	Rotary			Planar		
	SW_1	SW_2	SW_3	SW_4	SW_5	SW_6
0°	0	0	1	0	1	0
120°	1	0	0	1	0	0
240°	0	1	0	0	0	1

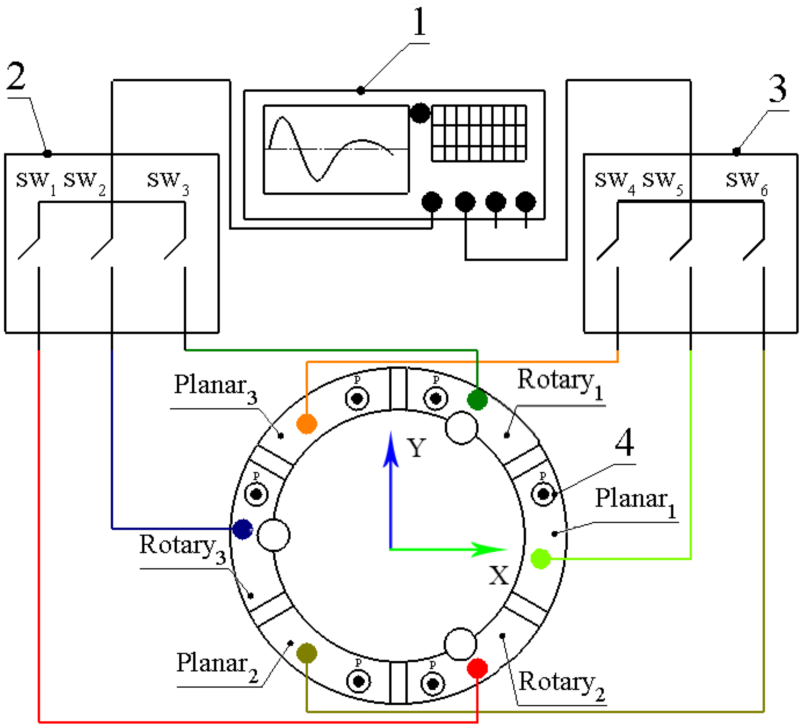

Figure 3. Excitation schematics of the actuator; 1—signal generator; 2—switching box used for angular motion control; 3—switching box used for linear motion control; 4—polarization direction of piezoceramic ring.

It must be noted that both rotary and planar motions can be generated by combining two excitation signals. In addition, motion trajectory planning algorithms can be applied to obtain complex motion trajectories [24]. Amplitudes of the electric signal, sequences of switching electrodes, are used as outputs of the trajectory control algorithms. Moreover, the burst type signal or DC signal can be used to obtain higher output forces or increase the resolution of the motion.

3. Numerical Investigation of the Actuator

Numerical modeling of the actuator was performed to obtain suitable modal shapes, to analyze electrical and mechanical characteristics of the actuator, and to study vibrations of the contacting elements while a single electrode is affected by the excitation signal. Comsol Multiphysics 5.4 was used to build the numerical model. Geometric dimensions were set as shown in Table 1. Material properties used to build the model are shown in Table 3. C17200 beryllium bronze was used for the cylindrical part of the actuator, piezoelectric characteristics were set for the ring, and finally, alumina oxide properties were used for spherical contacting elements (Figure 1). Boundary conditions were set as follows: gravity force was included, the model was analyzed as a mechanically free system, and short circuit electric boundary conditions were used during modal-frequency analysis.

Table 3. Material properties.

Material Properties	Beryllium Bronze C17200	PI Ceramics PIC181	Aluminum Oxide Ceramic
Density, [kg/m^3]	8360	7800	3980
Young's modulus, [N/m^2]	10×10^9	7.6×10^{10}	41.9×10^{10}
Poisson's coefficient	0.34	-	0.33
Isotropic structural loss factor	0.02	-	0.2×10^{-3}
Relative permittivity	-	$\varepsilon_{11}{}^T/\varepsilon_0 = 1200$ $\varepsilon_{33}{}^T/\varepsilon_0 = 1500$	-
Elastic compliance coefficient [10^{-12} m^2/N]	-	$S_{11}{}^E = 15.00$ $S_{33}{}^E = 19.00$	-
Elastic stiffness coefficient $c_{33}{}^D$, [N/m^2]	-	1.6×10^{10}	-
Piezoelectric constant d_{33} [10^{-12} m/V]	-	225	-
Piezoelectric constant d_{31} [10^{-12} m/V]	-	−97	-
Piezoelectric constant d_{15} [10^{-12} m/V]	-	330	-

Firstly, modal-frequency analysis of the actuator was performed to identify modal shapes that can be used for achieving planar and rotational motions. The spherical payload was substituted by the distributed load placed on the three spherical contacts located on the top of the piezo ceramic ring.

Suitable vibration modes were found at the frequencies of 18.02 kHz and 46.199 kHz (Figure 4). It can be seen that vibrations of individual parts of the actuator occur as different vibration modes. Three supports have radial vibrations at the frequency of 18.02 kHz that can be used to induce planar motion of the actuator. The third radial vibration mode of the piezoceramic ring is obtained at the frequency of 46.199 kHz and can be used to rotate the payload. It must be noted that there is loose coupling between vibrations of the spherical contacts located at the top and bottom of the actuator when the actuator vibrates at these two modes. Therefore, it will be possible to excite planar and angular movements independently.

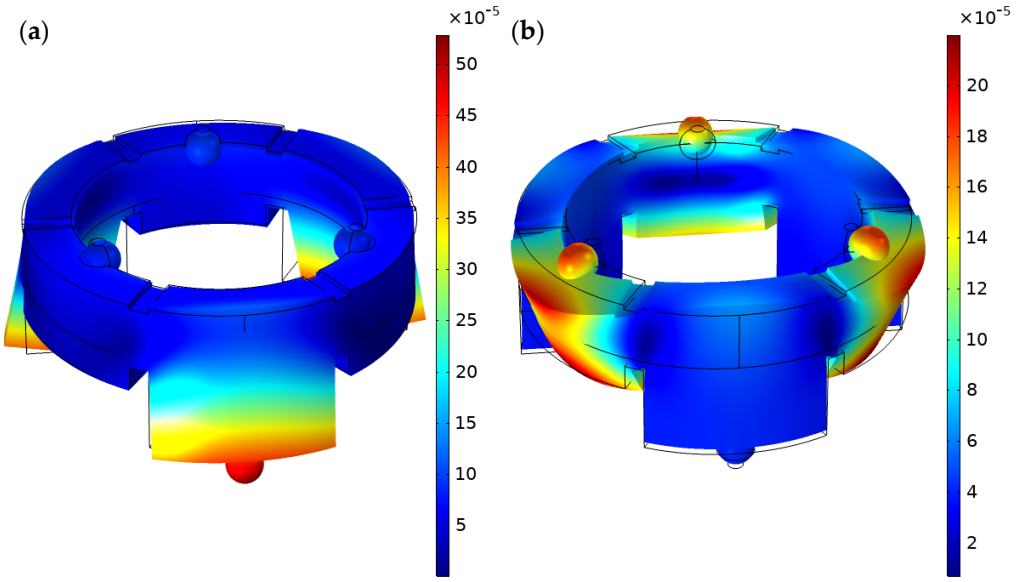

Figure 4. Modal shapes of the actuator: (**a**)—the first radial mode (18.02 kHz); (**b**)—the third radial mode of the piezoceramic ring (46.199 kHz).

The next step of the numerical investigation was the analysis of impedance-phase-frequency characteristics with the goal of indicating operation frequencies of the actuator. The calculations were performed at the following electrical boundary conditions: the electrode dedicated to angular or linear motion control was affected by excitation voltage of

100 $V_{p\text{-}p}$ while remaining electrodes were set to open-circuit conditions. Results are given in Figure 5. It can be seen that resonant frequencies of the first radial and the third radial modes are obtained at 18.01 kHz and 46.172 kHz, respectively. Minor differences between natural and resonant frequencies occur due to slight differences in electrical boundary conditions. It can be seen that phase change at the resonant frequency is 12.1 degrees and 1.9 degrees (Figure 5). This means the corresponding vibration modes have relatively low efficiency.

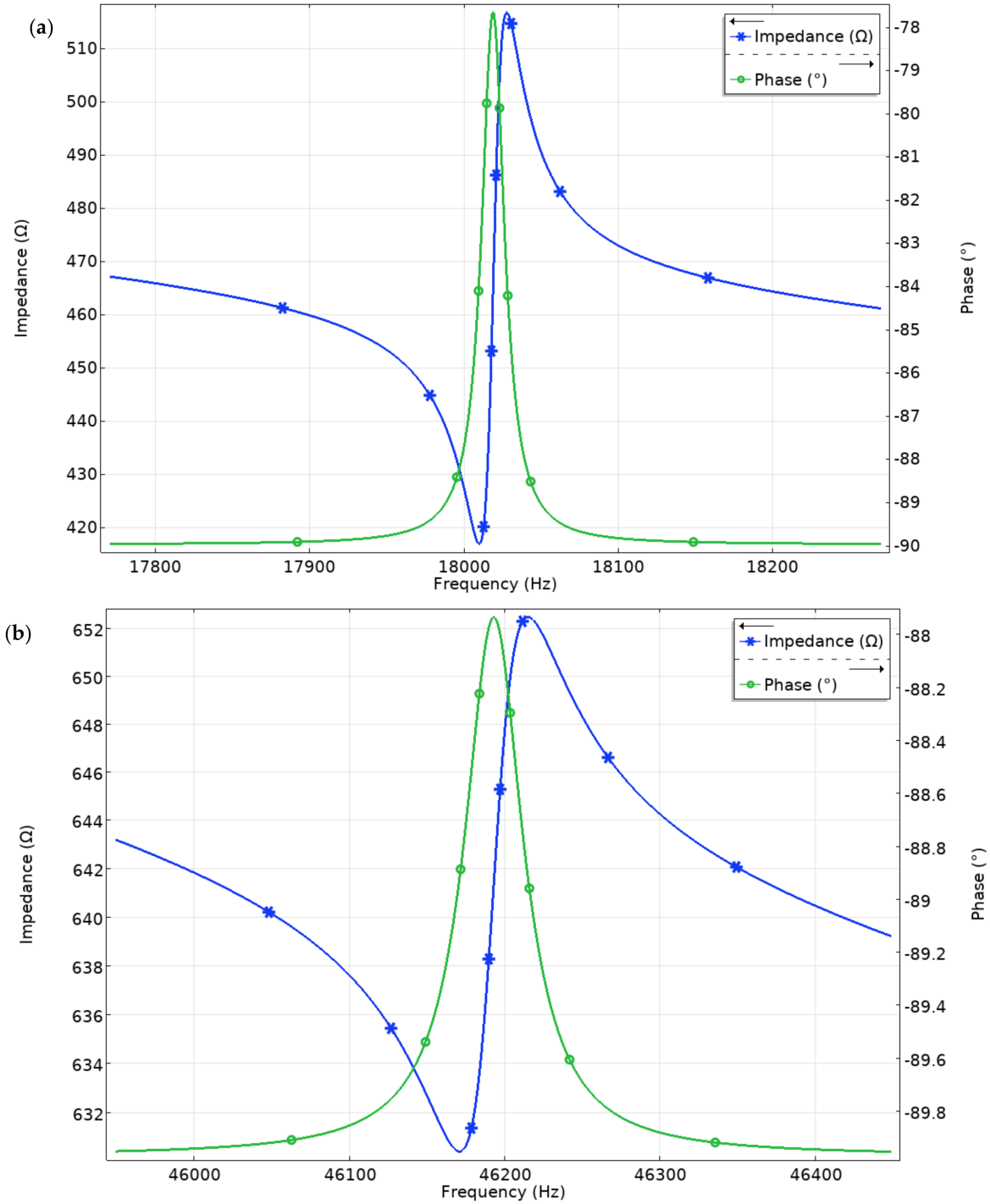

Figure 5. Impedance and phase characteristics in the frequency range of 17.76–18.29 kHz (**a**) and 45.96–46.46 kHz (**b**).

Harmonic response analysis also was performed to analyze amplitudes of contacting points vibration. The calculations were made when the voltages of 50 V_{p-p} and 200 V_{p-p} were applied for both modes. A single electrode was excited. Coupling between vibrations of different contact points was analyzed as well. Figure 6a shows that the highest displacement amplitude was obtained at a frequency of 18.017 kHz. The frequency value is in good agreement with the results of impedance frequency analysis. Also, it can be seen that the contact point located at the support under the excited electrode ($Planar_1$) has the highest displacement of 3.91 µm. The ratio between displacement amplitude and applied voltage is 78.2 nm/V_{p-p}. On the other hand, it can be observed that contact points located on the passive segments ($Planar_2$ and $Planar_3$) generate notably lower displacement amplitudes, i.e., 380 nm and 340nm. In addition, contact points located on segments for angular motion, $Rotary_1$–$Rotary_3$, also vibrate with amplitudes of 183 nm, 151 nm, and 136 nm, respectively. The coupling ratio between vibration amplitudes of excited and passive planar segments does not exceed 11.5 times and is not more than 28.75 times between excited segment and passive segments of angular motion. Figure 6b represents the displacement-frequency characteristics of the actuator while excitation signal amplitude was set to 200 V_{p-p} and was applied on electrode $Planar_1$. The highest displacement amplitude of the active segment reached 15.61 µm or 78.05 nm/V_{p-p}. The contact points located on $Planar_2$ and $Planar_3$ segments have amplitudes of 3.81 µm and 3.45 µm, respectively. Therefore, the ratio between active and passive planar segments is 4.52 times. Analyzing vibration amplitudes of contact points located on $Rotary_1$–$Rotary_3$ segments, it can be seen that it reaches 751 nm, 648 nm, and 557 nm, respectively. The coupling ratio of vibrations amplitudes is around 21 times in this case. Therefore, coupling between vibrations increases when excitation voltage increases as well. This means that when high voltage is applied, it will be complicated to achieve the planar and rotational motion of the payload independently. The same studies were performed for contact points driven by $Planar_2$ and $Planar_3$ segments in order to fully investigate displacement amplitudes and indicate vibrations coupling between all actuator segments while 200V_{p-p} is applied. A summary of the investigation is given in Figure 7.

As can be found in Figure 7a, displacement amplitudes of contact points are similar, and differences of displacement amplitudes do not exceed 9.5%. In addition, it can be found that coupling ratios between planar segments are similar in all cases. On the other hand, displacement amplitudes of contact points located on rotary segments (Figure 7b), are low and ensure high coupling ratios i.e., up to 24.6 times. Therefore, it can be stated that the vibrations of passive planar segments will have a minor influence on motion direction when excitation of planar motion is used, and rotary segments will be almost at rest at the same conditions. Investigation of displacement amplitudes of all contacting points and vibration coupling ratio while single segment $Rotary_1$ is affected by excitation signal was performed as well. Two studies were performed at different frequency ranges while the amplitude of excitations signal was set to 50 V_{p-p} and 200 V_{p-p}. Results of calculations are given in Figure 8.

The maximum displacement amplitudes were obtained at a frequency of 46.18 kHz. It confirms the results of impedance and phase-frequency characteristics calculations. The maximum displacements of 5.92 µm and 23.15 µm were obtained when excitation voltage of 50 V_{p-p} and 200 V_{p-p} were amplitudes to segment $Rotary_1$, respectively. The ratio between displacement amplitude and applied voltage is 118.4 nm/V_{p-p} and 115.7 nm/V_{p-p}, respectively. The coupling ratio between vibrations of rotary segments is up to 4.19 times when 50 V_{p-p} was applied and 4.1 times when 200 V_{p-p} was applied. It can be seen that the coupling ratio of vibrations between rotary segments is similar at different excitation voltages. Moreover, the coupling ratio of vibrations between rotary and planar segments is up 17.4 times while 50 V_{p-p} was applied and up to 17.14 times while 200 V_{p-p} was applied. In order to fully investigate the coupling ratio, the numerical investigation was performed when rotary segments $Rotary_2$ and $Rotary_3$ were affected by 200 V_{p-p}. A summary of the investigations is given in Figure 9.

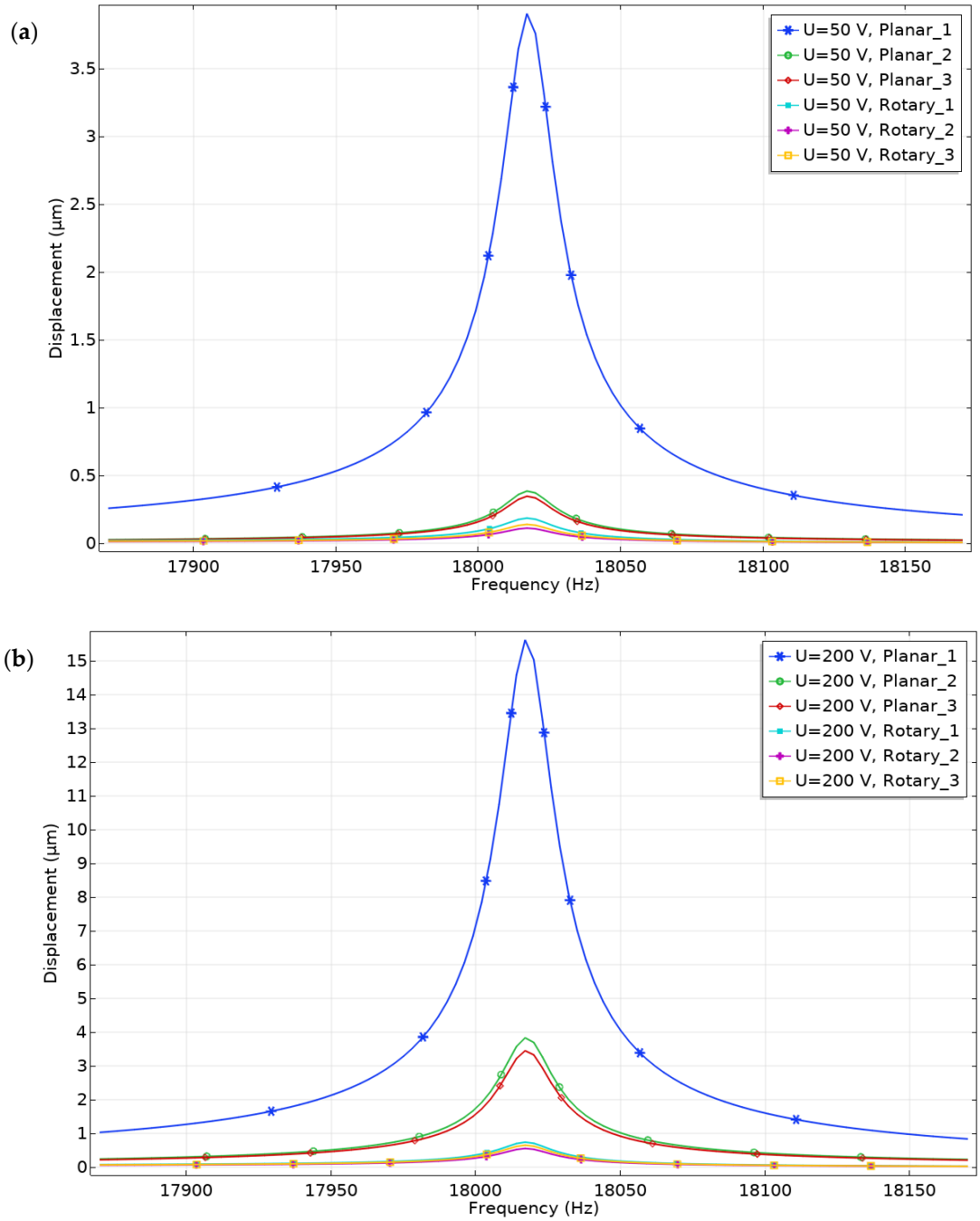

Figure 6. Displacement—frequency characteristics of six spherical contacts when segment $Planar_1$ is excited by the voltage of 50 $V_{p\text{-}p}$ (**a**) and 200 $V_{p\text{-}p}$ (**b**).

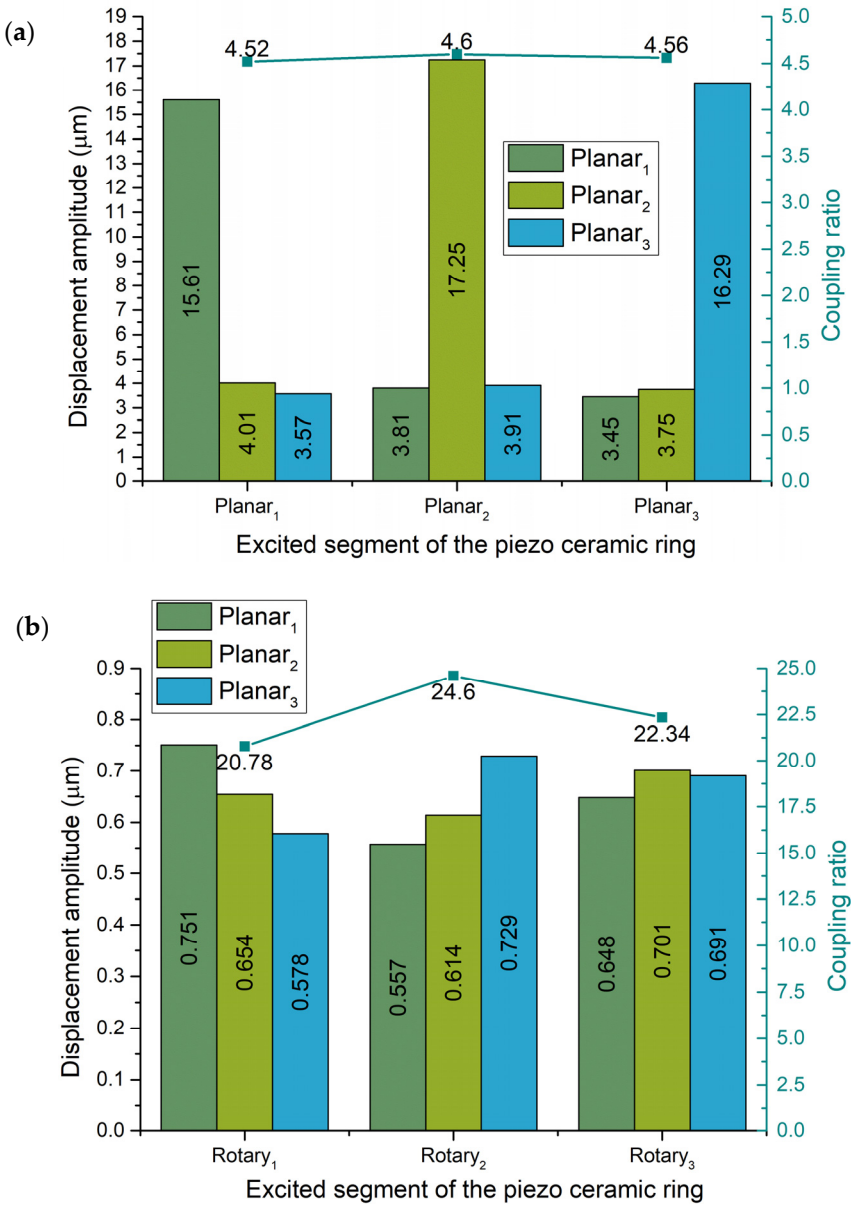

Figure 7. Comparison of spherical contacts displacement amplitudes and coupling ratios located in planar segments (**a**) and rotary segments (**b**) when different planar segments are excited by the voltage of $200V_{p\text{-}p}$.

As can be found in Figure 9a, displacement amplitudes of all contact points located on rotary segments are similar. The differences do not exceed 6.16%, while vibrations coupling ratios are also almost the same. The difference in the coupling ratio does not exceed 11%. Therefore, it can be stated that the influence of coupling vibrations between rotary segments will have a minor influence on angular motion direction. In addition, considering to results represented in Figure 9b, it can be found that the coupling ratio between rotary and planar segments is up to 17.39 times, while fluctuations between coupling ratio values do not exceed 6.15%. Therefore, it can be assumed that during the excitation of angular motion, the actuator will not generate planar motion and will stay in a constant position.

Motion trajectories of contact spheres at the resonant frequencies of 18.017 kHz and 46.199 kHz were studied as well. Time-domain studies were set for both vibrations modes. Time ranges were set to one period of vibrations (T). Excitation voltage amplitude was set to 200 $V_{p\text{-}p}$ for both cases. Electrodes located on segments $Rotary_1$ and $Planar_1$ were affected by excitation voltage separately, while other segments were set to open-circuit conditions.

Results of calculations are given in Figure 10. It can be seen that motion trajectories have almost linear trajectories in both cases. The projection of the motion trajectory in the *Y*-axis is 22.34 µm, while the projection in *X*-axis is 7.18 µm (Figure 10a). The length of the trajectory is 23.47 µm. Projection of angular motion trajectory of contact sphere motion reached 8.8 µm and 15.61 µm in *Y* and *Z* axes, respectively. The length of the trajectory is 17.92 µm.

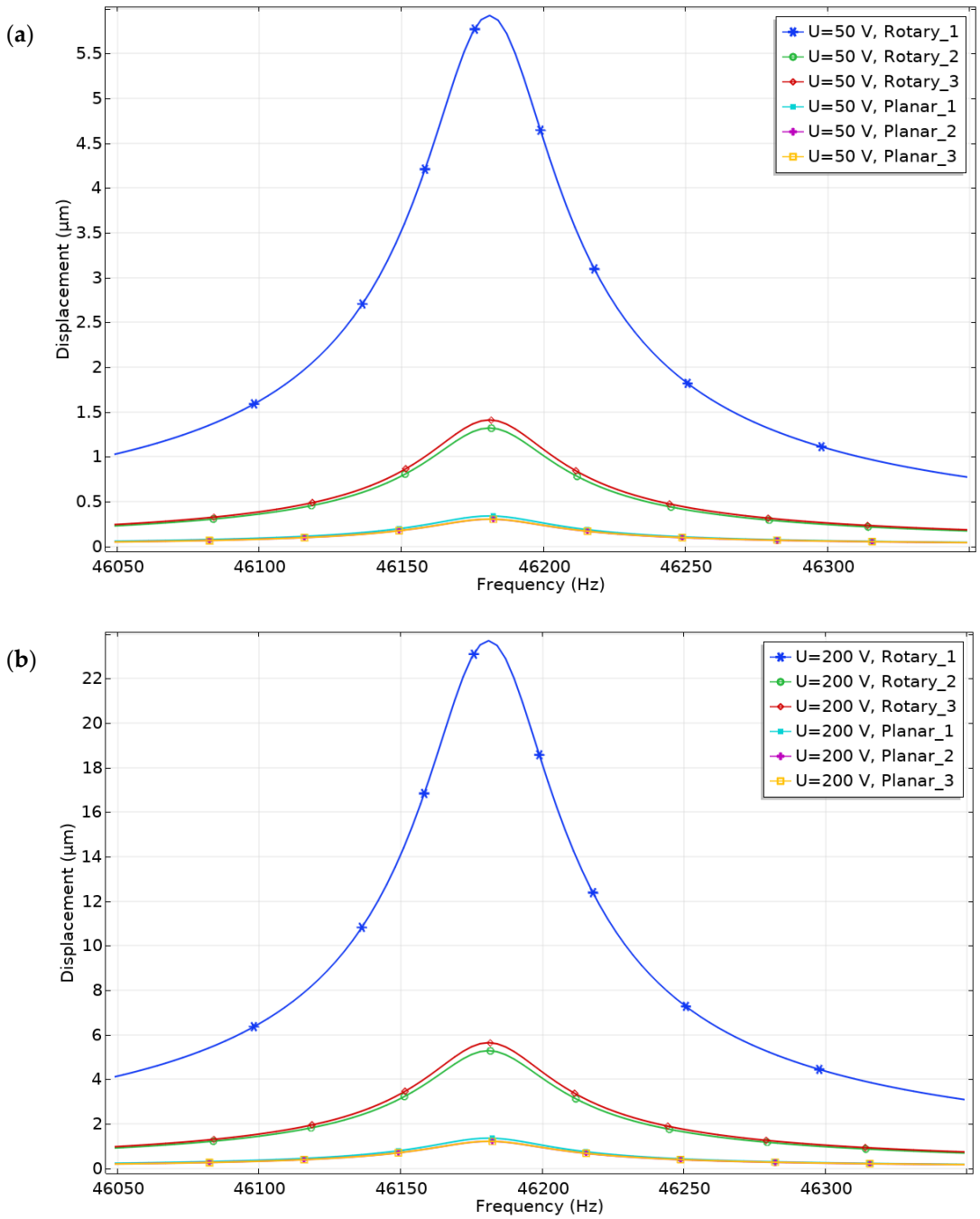

Figure 8. Displacement—frequency characteristics of six spherical contacts when segment $Rotary_1$ is excited by the voltage of 50 $V_{p\text{-}p}$ (**a**) and 200 $V_{p\text{-}p}$ (**b**).

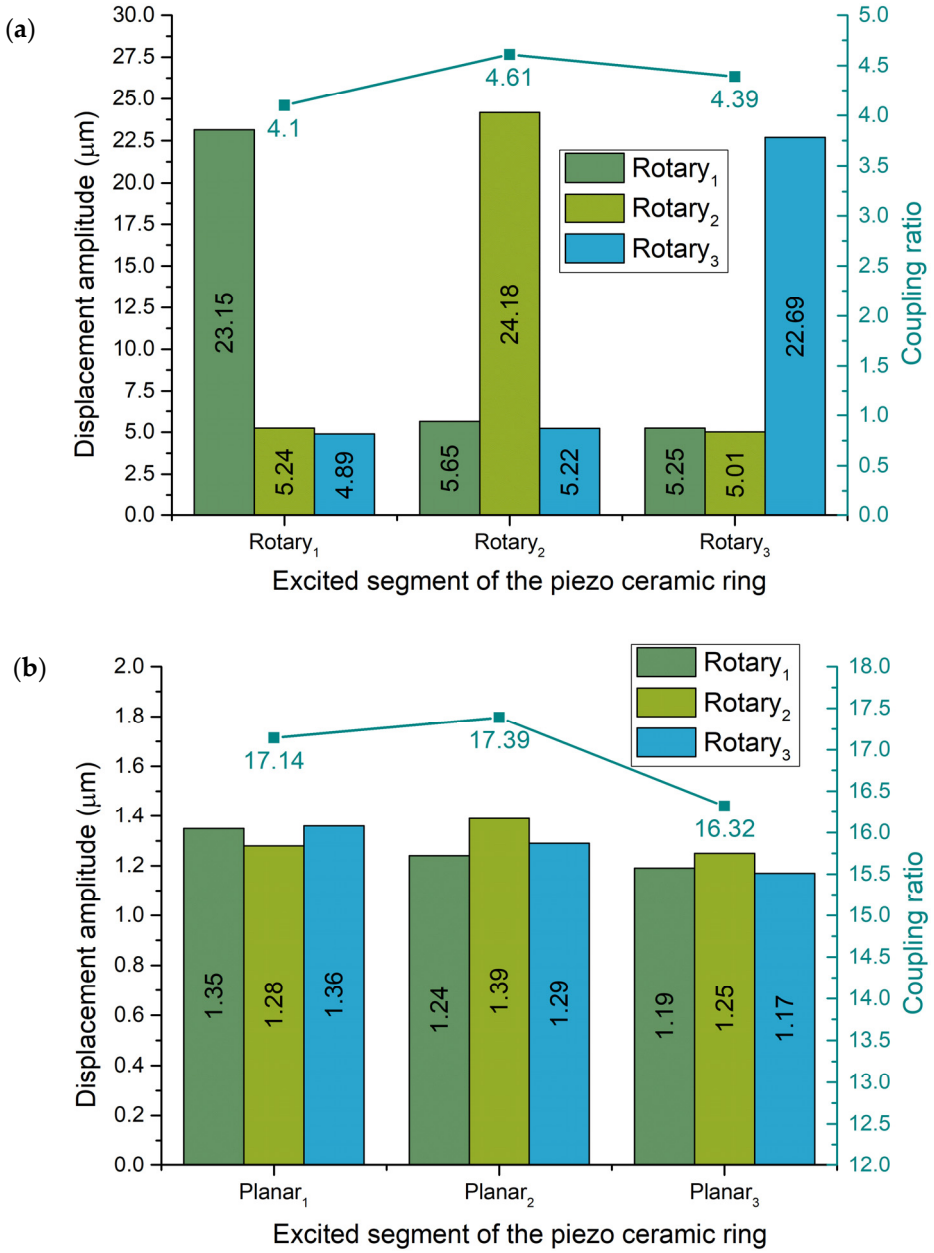

Figure 9. Comparison of spherical contacts displacement amplitudes and coupling ratios located in rotary segments (**a**) and planar segments (**b**) when corresponding rotary segments are excited by the voltage of 200 $V_{p\text{-}p}$.

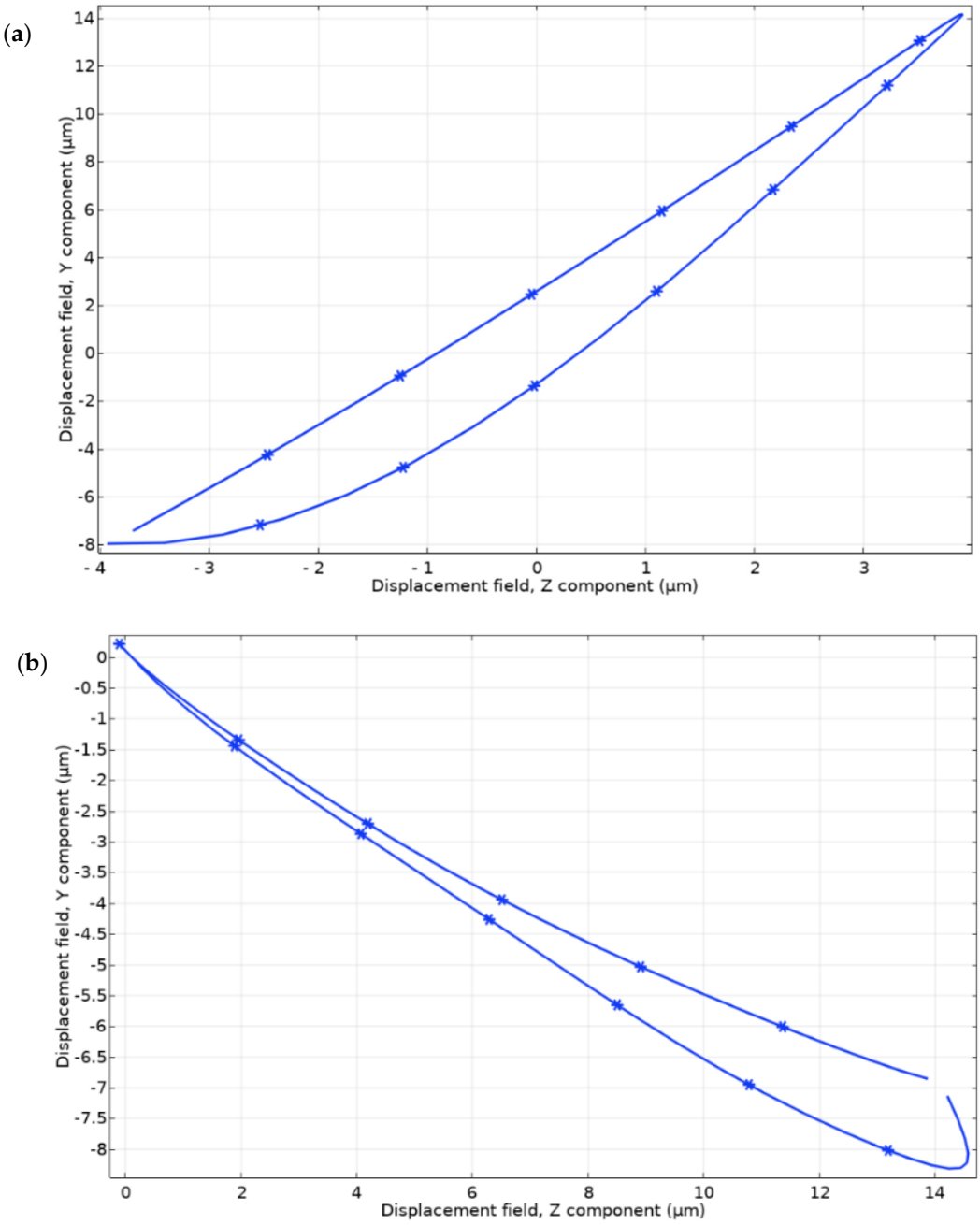

Figure 10. Contact points trajectories when segment $Planar_1$ (**a**) and segment $Rotary_1$ (**b**) is exited by the voltage of 200 $V_{p\text{-}p}$.

4. Experimental Investigation of the Actuator

The prototype of the actuator was made to perform experimental investigations (Figure 11). The geometric and physical characteristics of the prototype correspond to the characteristics used for numerical investigations.

Firstly, impedance—frequency characteristics of the actuator were measured using SinPhase 16777k (SinPhase, Mödling, Austria) impedance analyzer. The actuator was placed on the foam, and measurements were performed without payload. Firstly, the impedance analyzer was connected to $Planar_1$, while other segments were set to open circuit condition. The same measurement was performed while $Rotary_1$ was connected to the analyzer. The results are shown in Figure 12.

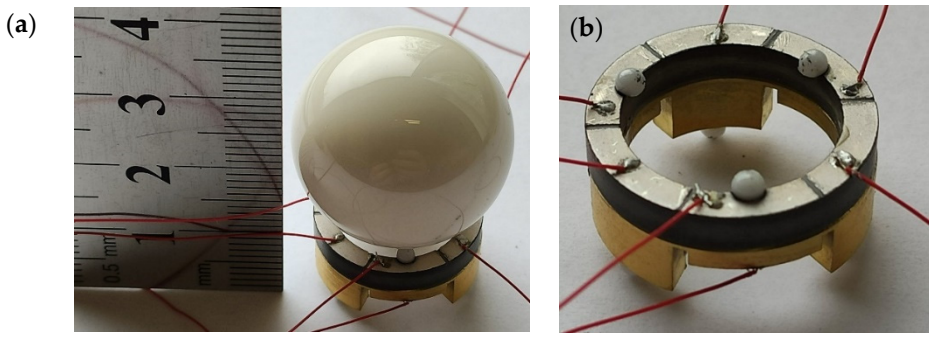

Figure 11. Prototype of the actuator with spherical payload (**a**) and without payload (**b**).

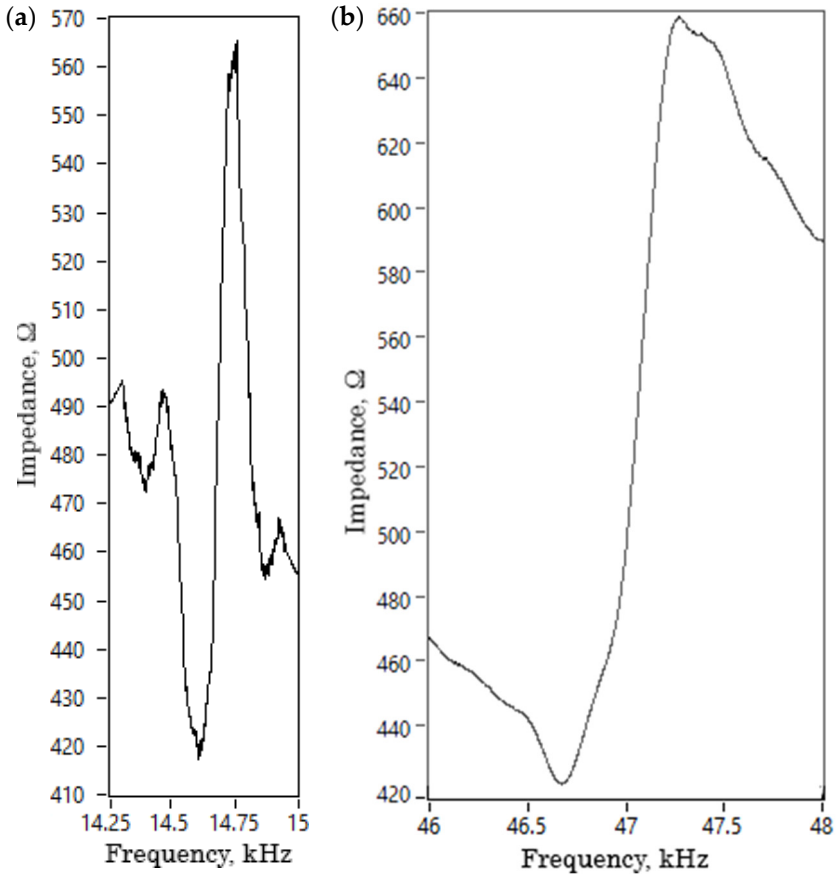

Figure 12. Measured impedance—frequency characteristics of the actuator in the frequency range of 14.25–15.00 kHz (**a**) and 46.0–48.0 kHz (**b**).

It can be seen that the resonant frequency of the actuator was obtained at frequencies of 14.67 kHz and 46.62 kHz. The differences between calculated and measured frequencies do not exceed 1.5% for a radial mode of piezoceramic ring. On the other hand, the difference between calculated and measured resonant frequencies of the first radial mode of actuator supports is 3.34 kHz or 18.5%. The difference mainly comes because of different mechanical boundary conditions used during measurements and manufacturing errors. The quality factor of the actuator when it vibrates at operating frequencies is Q_{planar} = 983.14; Q_{rotary} = 1014.5. The difference between impedance values at the resonant and anti-resonant frequencies is up to 260 Ω. It is mainly affected by the specific design of the actuator.

Dynamic characteristics of the actuator were measured at different excitation conditions. The experimental setup was built and is shown in Figure 13. The experimental setup consisted of a computer, a function generator WW5064 (Tabor Electronics, Nesher,

Israel), a power amplifier PX-200 (Piezo Drive, Shortland, Australia), oscilloscope DL2000 (Yokogawa, Tokyo, Japan), a displacement sensor ILD 2300 (Micro-Epsilon, Ortenburg, Germany), tachometer DT210 (Nidec-Shimpo, Nagaokakyo-City, Japan) and a self-made switch box.

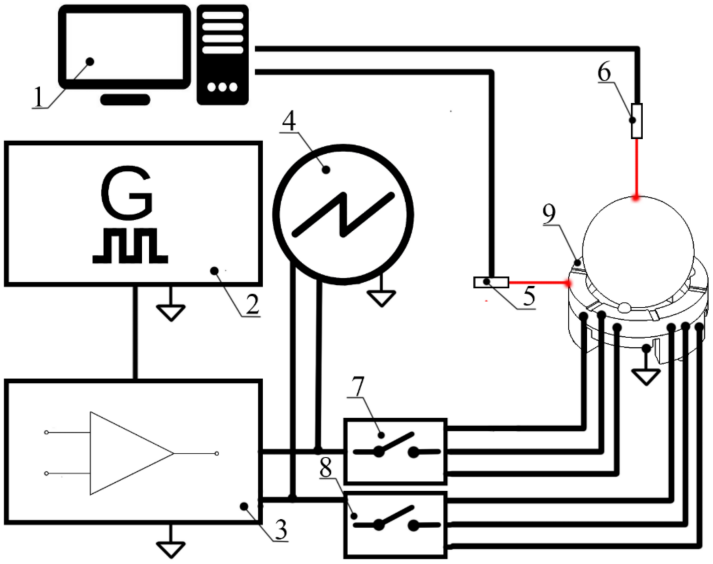

Figure 13. Schematics of the experimental setup: 1—computer; 2—signal generator; 3—power amplifier; 4—oscilloscope; 5—displacement sensor; 6—tachometer; 7—switch box for planar motion control; 8—switch box for angular motion control; 9—the prototype of the actuator.

The actuator was placed on the flat glass surface, and the planar velocity of the actuator was measured. Excitation voltage varied from 80 $V_{p\text{-}p}$ to 200 $V_{p\text{-}p}$, and a payload of 12.6 g, 25.1 g, and 55.68 g was applied. Firstly, measurements were made while the electrode located in segment $Planar_1$ was excited while other electrodes were set to open-circuit conditions. The payload of the actuator was changed manually by replacing the spherical payload. Results of the measurement are shown in Figure 14.

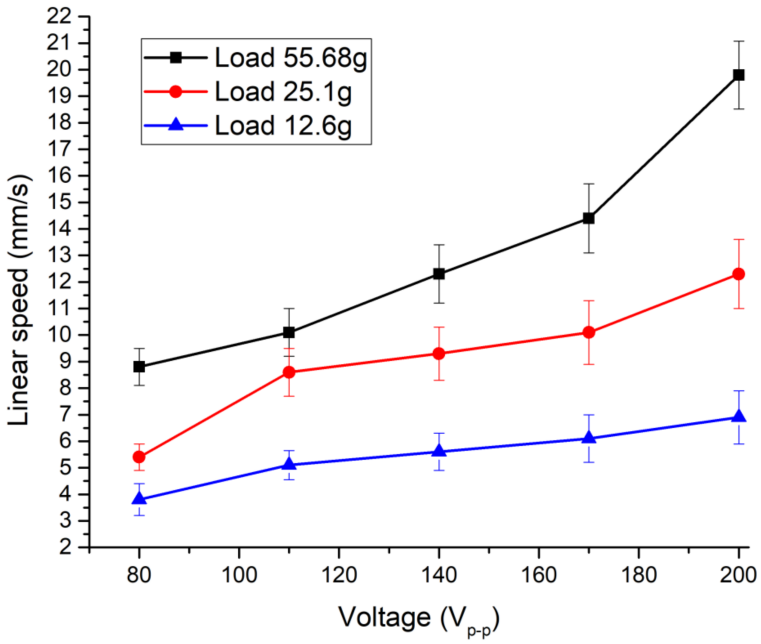

Figure 14. The measured linear velocity of the actuator at the different preloads when segment $Planar_1$ of the actuator is excited.

The lowest and highest velocities of the actuator were obtained at 80 V_{p-p} and 200 V_{p-p}, respectively. The lowest velocity values reached 3.8 mm/s at 12.6 g, 5.4 mm/s at 25.1 g and 8.8 mm/s at 55.68 g, while the highest reached 6.9 mm/s, 12.3 mm/s and 19.8 mm/s, respectively. It can be noted that velocity characteristics are almost linear increases when voltage is increasing. Also, a higher preload value causes higher velocity because of the increment of friction force between surface and contact spheres. More detailed measurements of the planar velocity were made when electrodes located in segments $Planar_2$ and $Planar_3$ were excited. Comparison of the measured maximum and minimum velocities at different payloads are given in Figure 15. It can be seen that velocities have minor differences at different payloads when the voltage of 80 V_{p-p} and 200 V_{p-p} is applied. The difference value does not exceed 9.49%. It shows that the actuator is able to provide stable planar motion characteristics in different directions at different payload values. The highest velocities of 8.8 mm/s, 8.6 mm/s, and 8.3 mm/s were obtained when a payload of 55.68 g and voltage of 80 V_{p-p} were applied on corresponding electrodes (Figure 15a). On the other hand, the highest velocities of 19.8 mm/s, 18.8 mm/s, and 19.6 mm/s were obtained when the voltage of 200 V_{p-p} was applied, and a payload of 55.68 g was used. Video S1 was included to supplementary materials in order to represent planar motion of robot.

Angular velocity of the spherical payload was measured at different values of payload and excitation voltage values. Three different electrodes located in the segments $Rotary_1$–$Rotary_3$ were affected by harmonic voltage in the range of 80 V_{p-p} to 200 V_{p-p}. Firstly, angular velocities generated by contact located on segment $Rotary_1$ were investigated. The payloads values were the same as in previous measurements. The results are shown in Figure 16.

The lowest angular speed of 4.8 RPM, 8.5 RPM, and 12.4 RPM was obtained at 80 V_{p-p} when preload of 12.6 g, 25.1 g, and 55.68 g was applied. The highest angular speed values of 14.9 RPM, 24.7 RPM, and 31.3 RPM were obtained at 200 V_{p-p} at the same preload values. Also, it can be seen that angular speed is almost linearly increased when excitation voltage is increasing. Angular speed also depends on payload, i.e., the higher payload causes higher friction force and angular speed, respectively. Measurements of the angular velocity were also made when electrodes located in segments $Rotary_2$ and $Rotary_3$ were excited. A summary of the results is given in Figure 17.

It can be seen that angular speeds of spherical payloads generated by different segments at 80 V_{p-p} and 200 V_{p-p} excitation signals are similar, and the difference does not exceed 15.6%. The lowest angular speeds were obtained when 80 V_{p-p} excitation signal and payload of 12.6 g were applied to the actuator. The speeds reached values of 4.7 RPM, 5.1 RPM, and 4.3 RPM when electrode located in segment $Rotary_1$, $Rotary_2$, and $Rotary_3$ is excited, respectively. On the other hand, the highest angular speeds were obtained at a voltage of 200 V_{p-p} and payload of 55.68 g. The speeds reached values of 31.3 RPM, 29.8 RPM, 30.9 RPM from $Rotary_1$, $Rotary_2$, and $Rotary_3$ segments, respectively. The difference between angular velocities does not exceed 5%. It shows that the actuator can provide stable angular motion while different excitation signals and payloads are applied. Video S2 was included to supplementary materials in order to represent angular motion of payload.

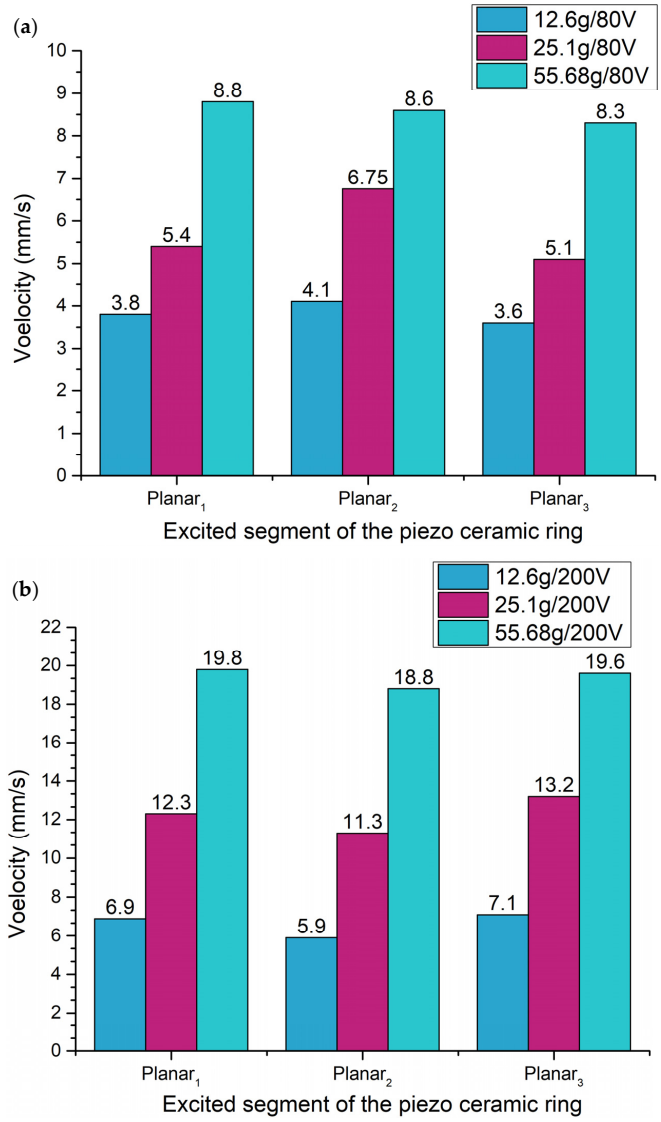

Figure 15. Comparison of the measured linear velocity of the actuator at the different preloads when the voltage of 80 $V_{p\text{-}p}$ (**a**) and 200 $V_{p\text{-}p}$ (**b**) is applied.

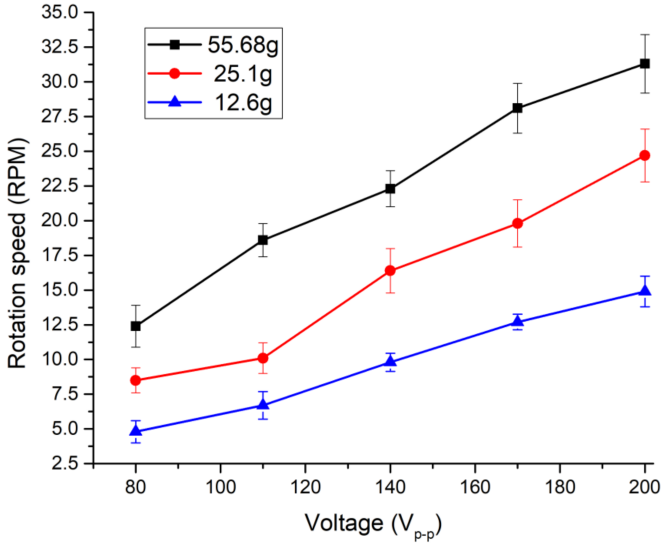

Figure 16. Measured rotational velocity at the different preload when segment $Rotary_1$ is excited.

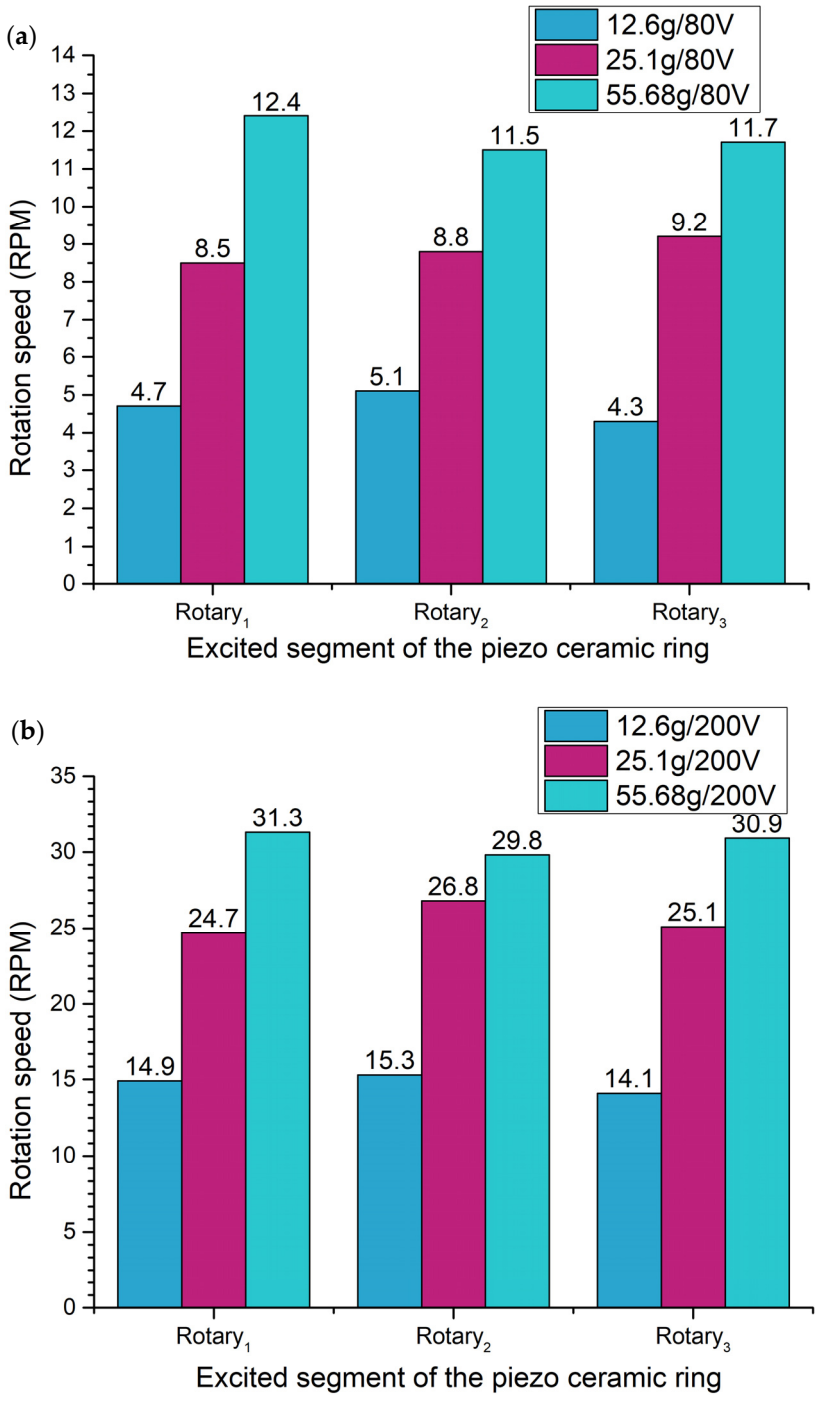

Figure 17. Comparison of the measured rotation speed at different payload when the voltage of 80 $V_{p\text{-}p}$ (**a**) and 200$V_{p\text{-}p}$ (**b**) is applied.

5. Conclusions

A novel design of a piezoelectric 5-DOF planar-angular actuator was introduced and investigated. The actuator has a simple structural design and can be scalable. Excitation of the actuator is based on a single harmonic signal, while control can be implemented using two digitally controlled switch boxes. Moreover, the design of the actuator allows reducing coupling between vibrations of the spherical contacts when planar or rotary motion is excited.

Numerical investigation showed that the first radial mode of the cylindrical actuator and the third radial mode of the piezo ceramic ring can be used to generate planar and

angular motions of the payload. Moreover, it was found that the vibration coupling ratio between segments related to planar motion is up to 4.56 times, and the coupling ratio with rotary segments is up to 24.6 times. On the other hand, during excitation of angular motion of payload vibration coupling ratio between rotary segments is up to 4.61 times, while the vibration coupling ratio between rotary and planar segments is up to 17.39 times. Therefore, excitation of angular and planar motions has a minor influence on each other.

Experimental investigations showed that maximum angular and planar motion characteristics reached 19.8 mm/s and 31.3 RPM, while a payload of 55.68 g and voltage of 200 $V_{p\text{-}p}$ is applied. Moreover, it was found that differences between motions characteristics at different payloads, motion directions, and excitation signals do not exceed 9.49% and 15.6% for angular and planar motions, respectively.

Supplementary Materials: The following are available online at: https://www.mdpi.com/article/10.3390/app12031033/s1; Video S1: represents the planar motion of actuator under payload; Video S2: represents the angular motion of actuator under payload.

Author Contributions: Conceptualization, D.M.; data curation, A.Č.; investigation, A.Č.; supervision, D.M.; validation, V.J.; visualization, V.J.; writing—original draft, A.Č. and V.J.; writing—review and editing, D.M. All authors have read and agreed to the published version of the manuscript.

Funding: This research was funded by the European Social Fund according to the activity "Promotion of postdoctoral fellowships studies" of Measure No. 09.3.3-LMT-K-712-19-0082.

Conflicts of Interest: The authors declare no conflict of interest.

References

1. Inamuddin, R.B.; Abdullah M., A. *Actuators: Fundamentals, Principles, Materials and Applications*; Scrivener Publishing: Beverly, MA, USA, 2020; pp. 1915–6106.
2. Yang, Z.; Zhang, L. Magnetic Actuation Systems for Miniature Robots: A Review. *Adv. Intell. Syst.* **2021**, *2*, 2000082. [CrossRef]
3. Naderi Rahnama, A.; Moghimi Zand, M.; Mousavi Mashhadi, M. An Analytical Investigation on the New Design of 3-DOF Flexible Nanopositioner Driven by Electrostatic Actuators. *Microsyst. Technol.* **2020**, *26*, 3737–3745. [CrossRef]
4. Niu, M.; Yang, B.; Yang, Y.; Meng, G. Modelling and Parameter Design of a 3-DOF Compliant Platform Driven by Magnetostrictive Actuators. *Precis. Eng.* **2020**, *66*, 255–268. [CrossRef]
5. Peng, H.; Wu, M.; Lu, H.; Wang, J.; Xiao, J.; Huang, Y.; Shi, D. A Distributed Strategy to Attitude Following of the Multi-DOF Parallel Electrical Manipulator Systems. *IEEE Trans. Ind. Electron.* **2021**, *46*, 1–10. [CrossRef]
6. Ghafarian, M.; Shirinzadeh, B.; Al-Jodah, A.; Das, T.K. Adaptive Fuzzy Sliding Mode Control for High-Precision Motion Tracking of a Multi-DOF Micro/Nano Manipulator. *IEEE Robot. Autom. Lett.* **2020**, *5*, 4313–4320. [CrossRef]
7. Liu, C.S.; Lin, Y.H.; Yeh, C.N. Analytical Investigation on Torque of Three-Degree-of-Freedom Electromagnetic Actuator for Image Stabilization. *Appl. Sci.* **2021**, *11*, 6872. [CrossRef]
8. Al-Jodah, A.; Shirinzadeh, B.; Ghafarian, M.; Kumar Das, T.; Tian, Y.; Zhang, D. A Fuzzy Disturbance Observer Based Control Approach for a Novel 1-DOF Micropositioning Mechanism. *Mechatronics* **2020**, *65*, 102317. [CrossRef]
9. Tian, X.; Liu, Y.; Deng, J.; Wang, L.; Chen, W. A Review on Piezoelectric Ultrasonic Motors for the Past Decade: Classification, Operating Principle, Performance, and Future Work Perspectives. *Sens. Actuators A Phys.* **2020**, *306*, 111971. [CrossRef]
10. Gao, X.; Yang, J.; Wu, J.; Xin, X.; Li, Z.; Yuan, X.; Shen, X.; Dong, S. Piezoelectric Actuators and Motors: Materials, Designs, and Applications. *Adv. Mater. Technol.* **2020**, *5*, 1900716. [CrossRef]
11. Zhang, S.; Liu, Y.; Deng, J.; Tian, X.; Gao, X. Development of a Two-DOF Inertial Rotary Motor Using a Piezoelectric Actuator Constructed on Four Bimorphs. *Mech. Syst. Signal Process.* **2021**, *149*, 107213. [CrossRef]
12. Gao, X.; Deng, J.; Zhang, S.; Li, J.; Liu, Y. A Compact 2-DOF Micro/Nano Manipulator Using Single Miniature Piezoelectric Tube Actuator. *IEEE Trans. Ind. Electron.* **2021**, *46*, 3928–3937. [CrossRef]
13. Niu, R.; Guo, Y. Novel Piezoelectric Crawling Robot with Multiple Degrees of Freedom. *AIP Adv.* **2021**, *11*, 075306. [CrossRef]
14. Gu, S.; Pan, P.; Zhu, J.; Wang, Y.; Yang, F.; Ru, C. A Piezoelectric Stick-Slip Drive Nanopositioner with Large Velocity under High Load. *AIP Adv.* **2020**, *10*, 105027. [CrossRef]
15. Lu, Q.; Chen, X. Application of Piezoelectric Actuator in Series Nano-Positioning Stage. *Sci. Prog.* **2020**, *103*, 1–14. [CrossRef]
16. Li, H.; Deng, J.; Zhang, S.; Yu, H.; Liu, Y. Design and Experiment of a Three-Feet Linear Ultrasonic Motor Using Third Bending Hybrid Modes. *Sens. Actuators A Phys.* **2021**, *331*, 112990. [CrossRef]
17. Hernando-García, J.; García-Caraballo, J.L.; Ruiz-Díez, V.; Sánchez-Rojas, J.L. Motion of a Legged Bidirectional Miniature Piezoelectric Robot Based on Traveling Wave Generation. *Micromachines* **2020**, *11*, 321. [CrossRef] [PubMed]
18. Su, Q.; Quan, Q.; Deng, J.; Yu, H. A Quadruped Micro-Robot Based on Piezoelectric Driving. *Sensors* **2018**, *18*, 810. [CrossRef] [PubMed]

19. Becker, F.; Minchenya, V.; Zimmermann, K.; Zeidis, I. Single Piezo Actuator Driven Micro Robot for 2-Dimensional Locomotion. In *Micromechanics and Microactuators*; Springer: Dordrecht, The Netherlands, 2011; Volume 2, pp. 1–10. [CrossRef]
20. Fan, P.; Liu, H.; Zheng, L. Study on a New Type of Miniature Piezo Walking Robot. *Smart Mater. Struct.* **2021**, *30*, 035023. [CrossRef]
21. Mashimo, T.; Toyama, S. Rotary-Linear Piezoelectric Microactuator. *IEEE Trans. Ultrason. Ferroelectr. Freq. Control* **2010**, *57*, 1825–1830. [CrossRef] [PubMed]
22. Tuncdemir, S.; Ural, S.O.; Koc, B.; Uchino, K. Design of Translation Rotary Ultrasonic Motor with Slanted Piezoelectric Ceramics. *Jpn. J. Appl. Phys.* **2011**, *50*, 027301. [CrossRef]
23. Han, L.; Yu, L.; Pan, C.; Zhao, H.; Jiang, Y. A Novel Impact Rotary-Linear Motor Based on Decomposed Screw-Type Motion of Piezoelectric Actuator. *Appl. Sci.* **2018**, *8*, 2492. [CrossRef]
24. Bansevicius, R.; Drukteiniene, A.; Kulvietis, G.; Tumasonienė, I. Design of Mobile Microrobot Based on Standing and Travelling Waves. *Int. J. Adv. Robot. Syst.* **2013**, *10*, 219. [CrossRef]